



Experimental Study on Aerodynamic Properties of Circulation Control Airfoil with Plasma Jet

Yanhua Zhang^(✉), Dengcheng Zhang, Lin Li, Wuji Zheng,
and Hao Luo

Aeronautics Engineering College,
Air Force Engineering University, Xi'an, China
angle0725@hotmail.com

Abstract. An experimental study on the circulation control around a modified NCCR1510-7067N airfoil is presented. The plasma-induced wall jet is achieved by the use of Dielectric Barrier Discharge plasma actuators, which are placed around the curved circular trailing edge. A wind tunnel test is performed in order to quantify the effects of applied voltage and actuator position on the lift enhancement. The lift and pressure measurements are taken using micro pressure electronic scanning valve. Additionally a smoke flow visualization test is performed in order to elucidate the fundamental working principles of the concept. Preliminary results indicate that the variation of the lift coefficient with the applied voltage was nonlinear, the short laminar separation bubble appeared at the leading edge in advance with applied voltages above 8 kV; consequently, the optimal applied voltage was 8 kV. The lift coefficient was increased by 0.154 and the lift augmentation efficiency reached 108.7 with a single actuator on the lower surface. A smoke flow visualization showed the delay of separation position and the formation of virtual flap effect.

Keywords: Plasma jet · Circulation control · Applied voltage · Lift · Coanda effect

1 Introduction

The development of mechanical high-lift systems as represented by flaps, ailerons, and various slats are relatively mature. However, such active control surfaces will increase the weight of the aircraft, the complexity of the structure, and cost of maintenance. Especially, many sharp-edged openings, protrusions, and other sources of possible radar detection caused by control surfaces will greatly reduce the stealth performance of aircraft. Therefore, the study on a novel high-lift system has become very important [1]. Circulation control technology [2] based on the Coanda effect [3] can delay boundary layer separation by injecting a tangential jet on the upper (lower) surface to flow along the blunt trailing edge. The airflow deflection driven by the tangential jet is equivalent to an increase of the effective pneumatic sinuosity of airfoil. Therefore, the circulation control technology has important research significance for improving both the short-range takeoff and landing (STOL) and stealth performance of an aircraft.

The conventional circulation control system [4] requires the gas source to generate the jet [5], and the power of the gas source is proportional to the square of aircraft takeoff speed [6], severely hindering the engineering application of circulation control technology [7, 8]. Consequently, this paper proposes the use of dielectric barrier discharge (DBD) plasma aerodynamic actuation [9] to produce the required jet for circulation control. The DBD plasma actuation system has a simple structure, does not require an additional gas source or any pipeline systems, and the flexible plasma actuator can generate tangential jet at any position around the circular trailing-edge of the airfoil, which is conducive to the formation of the Coanda effect.

In 2010, Zhang et al. [10] studied the effect of plasma actuator position on the lift characteristics of airfoil via numerical simulation. The lift augmentation efficiency can reach 134.86 at an angle of attack of 0 after actuation position optimization, which is much higher than the maximum lift augmentation efficiency of 80 for conventional jet circulation control. However, the effect of the plasma jet on the flow field was simulated through the volume force model hypothesis, and the results need be validated and supplemented by experimental data. In 2012, Wang et al. [11] conducted an experimental study of the plasma circulation control with a sharp trailing-edge airfoil, however, the lift augmentation efficiency could only obtain 9. In 2013 and 2014, Kotsonis et al. [12, 13] studied the effect of constant plasma actuation on the aerodynamic characteristics of an elliptic airfoil. The authors conducted a preliminary optimum selection of applied voltage and carrier frequency through wind tunnel experiments. However, no specific analysis was conducted for the action principle of different applied voltage on the aerodynamic characteristics of airfoil. Zhang et al. [14] studied the effect of several key parameters on plasma circulation control and found an optimal actuator position by numerical simulation. Yet, the results need be further verified by wind tunnel experiments.

In this paper, an experimental system of plasma circulation control was built, and the effect of different applied voltages and actuator positions near the airfoil trailing edge on the aerodynamic characteristics was studied in-depth. The optimal applied voltage and position of actuator were determined and the mechanism of plasma circulation control was revealed. In the experiment, the angle of attack (denoted by α) ranged from -4° to 12° , and the free stream velocity ranged from 6 m/s to 15 m/s. The research results provide the theoretical basis to reveal the optimal combination of key parameters of circulation control.

2 Experimental Setup

2.1 Wind Tunnel and Flow Measurements

The wind tunnel is a closed-loop circuit flow tunnel with a test section of $3\text{ m} \times 1.2\text{ m} \times 1.0\text{ m}$ (length \times width \times height). The test section speed ranges between 5 m/s and 75 m/s with turbulent intensity levels below 0.2%. The airfoil surface pressure was measured at 50 static pressure holes via 96-channel electronic micro pressure scanning valve with a range of ± 10 kPa. In the test, free stream velocities were selected by 6 m/s, 10 m/s, 15 m/s, and the angle of attack ranged from -4° to 12° , measured every 2° . The experimental system of the plasma circulation control is shown in Fig. 1.

To elucidate the fundamental principles of the plasma circulation control, a smoke flow visualization test was conducted. The test system included a diameter 0.1 mm nickel-cadmium wire and a variable voltage DC power supply (24 V, 10 A). Volatile glycerin was applied on the smoke-generating wire. Uniform smoke was generated when the wire was electrified, and filmed via digital camera above the airfoil, as shown in Fig. 2. The smoke-generating wire was horizontally arranged 0.2 m from the leading edge of the airfoil.

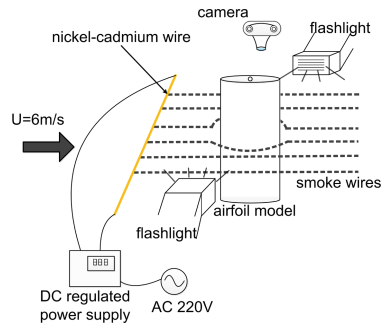
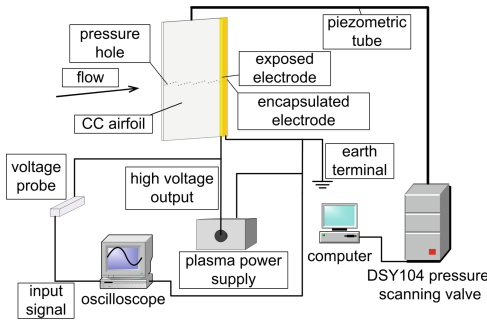


Fig. 1. Schematic of the experimental system of plasma circulation control **Fig. 2.** Smoke flow visualization system

2.2 Experimental Airfoil

The circulation control airfoil was derived from elliptic airfoil NCCR1510-7067N [15] with 15% chord thickness, 1% chord camber and modified blunt trailing edge. A ratio of 0.048 (Coanda surface radius to the chord length), determined via numerical optimization, has been shown to be conducive to the formation of the Coanda effect [16]. The airfoil profile and pressure holes distribution are shown in Fig. 3. The experimental wing model had a 0.3 m chord and a span of 1 m, and was vertically mounted on the wall of the wind tunnel. The model was made of steel structures, and the surface is covered with high-temperature resistant insulating Plexiglas to avoid interference between the steel frame and the surface discharge.

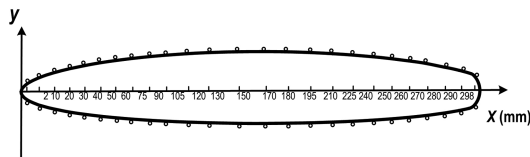


Fig. 3. NCCR 1510-7067N airfoil and distribution of the pressure holes

2.3 Plasma Actuator

The actuator was driven by CTP-2000 power supply (peak-to-peak voltage range 0–30 kV, actuation frequency range 6–25 kHz), and the electrical characteristic parameters of plasma actuation were measured through a DPO4104 oscilloscope, a P6015A high voltage probe, and a P6022 current probe. A typical asymmetric dielectric barrier discharge configuration was used. The actuators consisted of two rectangular electrodes with self-adhesive copper tape were used. The width of the exposed electrode was 3 mm, while the grounded electrode was 10 mm. The length of the electrodes was 1 m. No horizontal gap existed between both electrodes. The insulating polyimide tape with single layer thickness of 0.065 mm and a dielectric constant of 3.5 was selected as dielectric barrier, and the tape of 2 layers could endure the stability working voltage of 10 kV.

3 Results

The experimental results are mainly presented in the form of pressure coefficients and lift coefficients. The airfoil surface pressure coefficients were computed by dividing the pressure scanner output by the pitot-dynamic pressure.

$$C_P = \frac{p - p_\infty}{\frac{1}{2}\rho U^2} \quad (1)$$

In which p represents the static pressure of the measurement hole, obtained by the scanning valve. p_∞ , ρ and U represent the static pressure, the density and velocity of the free stream respectively. The lift coefficient C_L is given by:

$$C_L = \int_0^1 (C_p^u - C_p^l) d\left(\frac{x}{c}\right) \quad (2)$$

C_p^u and C_p^l represent the pressure coefficient of the upper and lower surfaces given by formula 1, x represents the position of the airfoil in the chord direction and c represents the chord length.

According to the lifting theorem $L = \rho U \Gamma$, if ρ and U are fixed, the lift L of the airfoil is proportional to the amount of circulation Γ around the airfoil. Circulation Γ is defined as the integral of the speed around the airfoil surface. The change of speed was influenced by the plasma jet, as well as the circulation and lift, which followed the basic principle of circulation control.

For plasma circulation control efficiency evaluation, the lift augmentation efficiency $\Delta C_L / C_\mu$ was imported. The momentum coefficient C_μ is given by:

$$C_\mu = \frac{M}{\frac{1}{2}\rho U^2 c} \quad (3)$$

The momentum induced by plasma actuation M is given by:

$$M = \int_0^h \rho v^2 dy \tag{4}$$

Where h and v represents the effective height and the velocity of the plasma jet at 6 mm behind the plasma actuator in quiescent air. By using the time resolution two-dimensional Partical Image Velocimetry (PIV) test, the flow field that was induced by the actuator in the static environment could be measured. Furthermore, the momentum was obtained by integrating the induced velocity, then, the momentum coefficient was calculated.

3.1 Effect of Applied Voltage on Lift Characteristics of Airfoil

The plasma actuator was designed and arranged at 295 mm in chord ($x/c = 98.3\%$) on the upper surface of the airfoil. High voltage electrode was at the front, and was followed by a low voltage electrode; both were separated by an insulating medium. The plasma jet was produced to accelerate the nearby airflow of the upper surface, shown in Fig. 4. The variation of the lift coefficient with applied voltage is shown in Fig. 5. The angles of attack were 2° , 4° , and 6° , the free stream velocities were 6 m/s and 10 m/s. The results showed that the lift remained basically unchanged, when the voltage was lower than 4 kV. At an angle of attack of 4° and a free stream velocity of 6 m/s, the lift coefficient increased most obviously. Furthermore, when the voltage was lower than 6 kV, the maximum slope of the lift coefficient with the applied voltage was 0.01506/kV. However, for a voltage above 6 kV, the maximum slope was 0.09981/kV. Therefore, the variation of the lift coefficient with the applied voltage was nonlinear, and the lift increased more rapidly with larger applied voltage. For example, the lift coefficient increased by 0.25 for an applied voltage of 10 kV. The reason is that the applied voltage directly affects the velocity and effective range of the plasma jet, for higher applied voltage, it is more convenient to drive the upper airflow to form the Coanda effect, leading to a more pronounced lift enhancement effect. When the applied voltage was fixed, the free stream velocity was lower, the jet was relatively stronger. therefore, the lift enhancement effect was better in the case of 6 m/s.

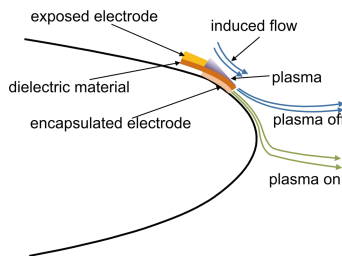


Fig. 4. DBD plasma actuator arranged at the circular trailing-edge of the airfoil

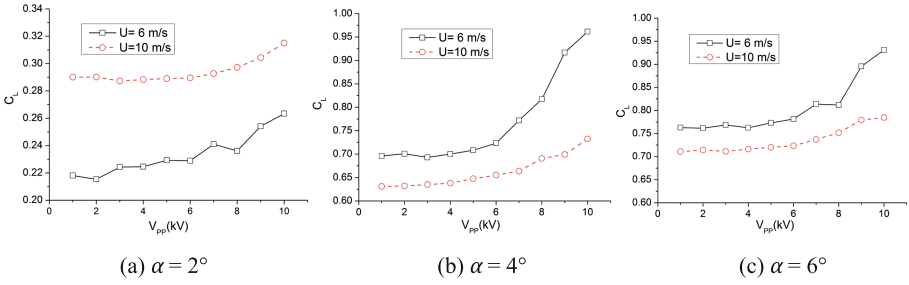


Fig. 5. Variation curves of the lift coefficient with the applied voltage at typical velocities and angles of attack

3.2 Effect of Applied Voltage on Laminar Separation Characteristics at Low Reynolds Number

The pressure distribution is shown in Fig. 6 for a free stream velocity of 6 m/s, according to low Reynolds number 1.3×10^5 . The suction on the upper surface and the pressure on the lower surface also increased. As a result, the circulation and lift of the airfoil increased. In addition, the pressure on the upper surface near the leading edge and trailing edge changed apparently. Due to the arrangement of the actuator at 98.3%, the last two pressure holes on the upper surface at 96.6% and 99.3% were covered. however, at the two holes (90% and 93.3) in front of the actuator, pressure decreased and flow velocity increased noticeably, indicating that there was a favorable pressure gradient between the front flow and the plasma zone. This is due to the increase of local velocity in the plasma zone.

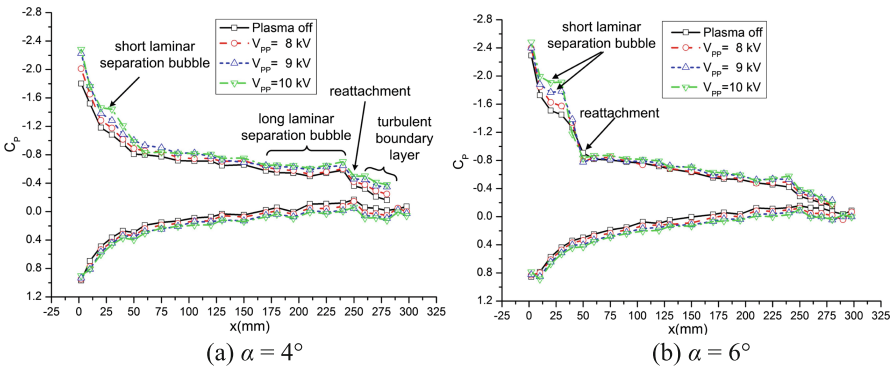


Fig. 6. Distribution of pressure coefficients at different velocities and angles of attack ($U = 6$ m/s)

Figure 6(a) shows a long pressure platform at 57%–80% chord on the upper surface, and a short pressure platform of 10 mm length near the leading edge with an applied voltage of 10 kV. Figure 6(b) shows a pressure platform of 20 mm length near the leading edge with applied voltages of 9 kV and 10 kV. This is directly related to the aerodynamic characteristics of airfoils at low Reynolds number. Numerous studies [17, 18] reported that the laminar separation phenomenon would appear at low Reynolds numbers. The pressure platforms shown in Fig. 7 corresponded to the formation of laminar separation bubbles, including long laminar separation bubble at 57%–80% chord and short laminar separation bubble near the leading edge.

For higher applied voltage, the larger circulation pushed the leading-edge stagnation point moving downward to the lower surface, and the flow in front of the stagnation point would move around the leading-edge to the upper surface against the adverse pressure gradient. Therefore, the boundary layer was easier to separate, leading to short laminar separation bubble. It can be seen for an applied voltage above or equal to 9 kV, a short laminar separation bubble appeared in advance and the flow field characteristics deteriorated. So 8 kV was chosen as the maximum applied voltage for all subsequent experiments. It has not been found that the plasma jet can inhibit the long laminar separation bubble on the upper surface in the experimental cases.

3.3 Effect of Actuator Position on Aerodynamic Characteristics of Airfoil

With the change of angles of attack, the separation point and the tail vortex position of the airfoil will change, and the effect of circulation control at different actuator positions will be significantly different. In consideration of the advantages of flexible actuator, which can generate tangential jet at any position around the circular trailing-edge of the airfoil. So the optimized design of the actuator positions can obviously improve the effect of the plasma circulation control.

Based on previous numerical simulations [19], eight actuator positions were set at 93.3%, 95%, 96.6% and 98.3% chord length on the upper surface, the trailing edge point and 98.3%, 96.6% and 95% on the lower surface, these were labeled as A, B, C, D, E, F, G and H respectively, as shown in Fig. 7. The high voltage electrode was positioned in front of the low voltage electrode on the upper surface, forming a backward plasma jet. Rather, it was arranged to form a forward induced jet on the lower surface.

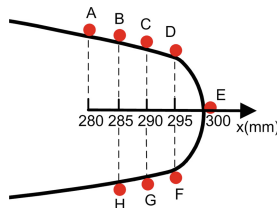


Fig. 7. Schematic diagram of the actuator position

Figure 8 shows the curves of lift coefficient increment versus angle of attack for different actuator positions on the upper surface, and the velocities are 6 m/s, 10 m/s and 15 m/s. Through PIV experiments and calculation, $C_{\mu} = 0.00151$ for 6 m/s, $C_{\mu} = 0.00054$ for 10 m/s and $C_{\mu} = 0.00024$ for 15 m/s, respectively. The results showed that the variation trend of the lift coefficient with the angle of attack as almost identical for all four positions, and the lift enhancement effect was most apparent at 6 m/s. In Fig. 8(a), For $\alpha = -4^{\circ}$ and -2° , the lift enhancement effect was better, and when the angle of attack changed from -2° to 6° , the effect was first weakened and then strengthened. beyond 6° , the effect gradually weakened. if an actuator position was at the front (positions A and B), the plasma jet was relatively far from the separation point, and the induced jet was not sufficiently strong to drive the inflow to form the Coanda effect, and the lift enhancement effect was weak. When the actuator gradually moved closer to the separation point (positions D), the induced plasma jet accelerated the upper surface airflow, forming an additional circulation. As a result, the separation point moved backward, and the streamline was deflected downward (shown in Fig. 10 (b)). At position D, the lift increment was higher than the other position from 3° to 12° . For a flow velocity of 6 m/s and an angle of attack of -2° , the lift coefficient increased by 0.122, which is equal in magnitude to Kotsonis et al., and the lift augmentation efficiency $\Delta C_L/C_{\mu} = 86.1$.

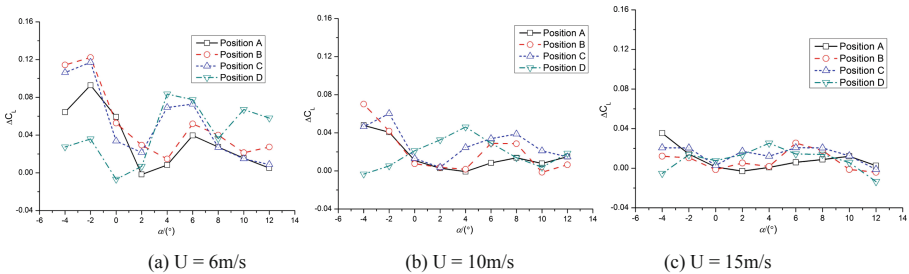


Fig. 8. Curves of lift coefficient increment versus angle of attack of different actuator positions on the upper surface and at different velocities

Figure 9 shows the curves of the lift coefficient increment versus the angle of attack at different actuator positions on the lower surface. The overall lift enhancement effect was significant at position F. When the flow velocity was 6 m/s with an angle of attack of 2° , the lift coefficient increased by 0.154, and the lift augmentation efficiency $\Delta C_L/C_{\mu} = 108.7$. This was much larger than the maximum value of 80 of the conventional circulation control, indicating the high efficiency of the plasma circulation control. In addition, as the velocity increased, the lift enhancement effect gradually weakened. In summary, the lift increment and the lift augmentation efficiency were better at position F than at the other positions on the upper or lower surfaces. This result is consistent with Zhang *et al.* and Kotsonis *et al.*

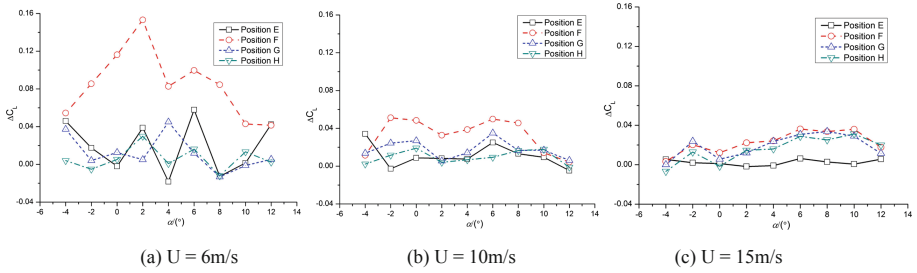


Fig. 9. Curves of lift coefficient increment versus angle of attack of different actuator positions on the lower surface at different velocities

As shown in Fig. 10, the four cases including plasma off, actuation at position D, actuation at position F, and the double actuations at position D and F combined, can be obtained with the smoke flow visualization test. In Fig. 10(c), Since the direction of the induced jet was contrary to the incoming flow, the jet obstructed the flow on the lower surface, which reduced the velocity, increased the pressure, and increased the lift. Furthermore, the plasma jet produced a significant counterclockwise vortex under the viscous effect. When the actuator position was at position F, both vortices were close, and their direction was identical, so they induced mutual coupling to form a larger vortex, leading to a clear bulge around the trailing edge. This significantly deflected the streamline downward and resulted in a similar flap effect, thus improving the lift enhancement effect. The effect was most apparent at $\alpha = 0^\circ - 2^\circ$, which was due to the downward separation vortex being relatively close to the induced vortex, this was beneficial for the interaction of both vortices. As previously reported [12, 13], a significant recirculation zone appeared on the lower surface near the trailing edge,

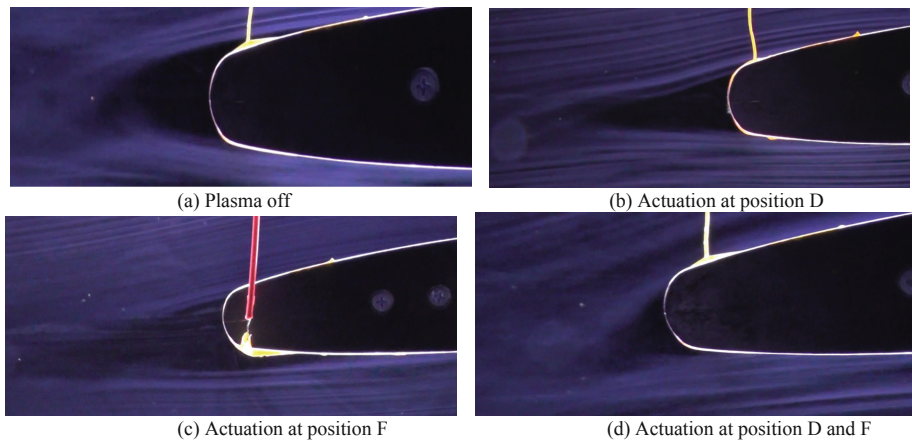


Fig. 10. The smoke flow visualization result for $\alpha = 0^\circ (U = 6 \text{ m/s})$

which creates the downward streamline, i.e., the virtual flap. In Fig. 10(d), the upper streamline was clearly deflected downward under the Coanda effect, and the overall streamline deflection was very obvious and the wake was also deflected downward, which is similar to the flow field of increasing airfoil sinuosity.

4 Conclusions

This paper presents an experimental study on the aerodynamic characteristics of the airfoil with presented plasma circulation control, analyzing two important factors: the applied voltage and the positions of the actuator. The effectiveness of the plasma circulation control used on the blunt trailing-edge airfoil was verified and a combination of optimal parameters was obtained.

With increasing applied voltage, the lift coefficient increased nonlinearly. The maximum increment of the lift coefficient was 0.25 at 4° with an applied voltage of 10 kV. This verified the apparent effectiveness and high efficiency of plasma circulation control. Long and short laminar separation bubbles existed on the upper surface at a free stream velocity of 6 m/s, according to the low Reynolds number of 1.3×10^5 . However the long laminar separation bubble was not inhibited by the plasma jet, and a short laminar separation bubble appeared in advance due to the leading-edge stagnation point downwards of the lower surface with applied voltages of 9 kV and 10 kV, therefore, the optimized applied voltage was 8 kV.

The better lift enhancement effect of the lower surface actuation appeared at position F, which was optimal among all selected positions. The maximum increment of the lift coefficient was 0.154 and the lift augmentation efficiency reached 108.7 at 2° . The action principle was that the counterclockwise-induced vortex coupled with the counterclockwise separation vortex in the separation region, leading to a bigger vortex and acting as a virtual flap like gurney flap. If the double actuators were excited at positions D and F at the same time, the series plasma jet could produce a more apparent Coanda effect.

The characteristics of high lift and high lift augmentation efficiency will be conducive for plasma circulation control. Furthermore, the plasma circulation control can overcome the bottleneck of the engineering application of gas resource and auxiliary power system that restricts traditional circulation control technology. Consequently, it has higher efficiency and better application prospect. However, the effective flow speed for applications still needs to be increased. Methods may include the optimization of plasma parameters, the improvement of penetration resistance of the dielectric barrier, and the application of a plasma synthetic jet, which will be investigated in a further study.

References

1. Zhu ZQ, Wu ZC (2016) Study of the circulation control technology. *Acta Aeronautica et Astronautica Sinica* 37(2):411–428
2. Montanya DL, Marshall DD (2007) Circulation control and its application to extreme short take-off and landing vehicles. In: *AIAA paper 2007*, p 1404
3. Coanda H (1936) Device for deflecting a stream of elastic fluid projected into an elastic fluid. U.S. Patent No. 2052869
4. Kanistras K, Saka PC, Valavanis KP et al (2015) Design and development of an air supply unit for circulation control wing-based UAVs. In: *IEEE aerospace conference, Big Sky, Montana*
5. Timo K, Vlad C, Ralf R, et al (2011) Active flow separation control on a high-lift wing-body configuration part 1: baseline flow and constant blowing. In: *AIAA*
6. Englar RJ (2004) Overview of circulation control pneumatic aerodynamics: blown force and moment augmentation and modification as applied primarily to fixed-wing aircraft. In: *Proceedings of the 2004 NASA/ONR circulation control workshop, part 1, NASA/Office of Naval Research*, pp 37–99
7. John LL (2004) Why have only two circulation-controlled STOL aircraft been built and flown in years 1974–2004. In: *Proceedings of the 2004 NASA/ONR circulation control workshop, part 2, NASA/Office of naval research*, pp 603–622
8. Fielding JP, Mills A, Smith H (2010) Design and manufacture of the DEMON unmanned air vehicle demonstrator vehicles. *J Aerosp Eng* 224(G):365–372
9. Wang JJ, Choi KS, Feng LH (2013) Recent developments in DBD plasma flow control. *Prog Aerosp Sci* 62:52–78
10. Zhang PF, Yan B, Liu AB et al (2010) Numerical simulation on plasma circulation control airfoil. *AIAA J* 48(10):2213–2226
11. Feng LH, Wang JJ, Choi KS (2013) Experimental investigation on lift increment of a plasma circulation control airfoil. *Acta Mech Sin* 45(6):815–821
12. Kotsonis M, Pul R, Veldhuis L (2013) Experiment study on airfoil circulation control using plasma actuators. In: *31st AIAA applied aerodynamics conference*, p 3164
13. Kotsonis M, Pul R, Veldhuis L (2014) Influence of circulation on a rounded-trailing-edge airfoil using plasma actuators. *Exp Fluids* 55:1772
14. Zhang YH, Li L, Zhang DC et al (2017) Aerodynamics of airfoil based on plasma circulation control. *High Power Laser Particle Beams* 29(6):065007
15. Abramson J (1977) Two-Dimensional Subsonic Wind Tunnel Evaluation of Two Related Cambered 15-Percent-Thick Circulation Control Airfoils, DTNSRDC TR
16. Corke TC, Enloe CL, Wilkinson SO (2010) Dielectric barrier discharge plasma actuators for flow control. *Annu Rev Fluid Mech* 42(1):505–529
17. Bai P, Li F, Zhan HL et al (2015) Study about the non-linear and unsteady laminar separation phenomena around the airfoil at low reynolds number with low incidence. *Sci Sin-Phys Mech Astron* 45:024703
18. Meng XS, Yang ZR, Chang Q et al (2016) Laminar separation control at low reynolds numbers using plasma actuation. *Acta Aeronautica et Astronautica Sinica* 37(7):2112–2122
19. Li L, Zhang DC, Zhang YH (2017) Numerical simulation study on interaction mechanism of plasma circulation control. *J Air Force Eng Univ* 18(3):9–16